

# Dual Mechanisms of Action of Self-Delivering, Anti-HIV-1 FANA Oligonucleotides as a Potential New Approach to HIV Therapy

Mayumi Takahashi,<sup>1</sup> Haitang Li,<sup>1</sup> Jiehua Zhou,<sup>1</sup> Pritsana Chomchan,<sup>1</sup> Veenu Aishwarya,<sup>2</sup> Masad J. Damha,<sup>3</sup> and John J. Rossi<sup>1,4</sup>

<sup>1</sup>Department of Molecular and Cellular Biology, Beckman Research Institute, City of Hope, Monrovia, CA 91016, USA; <sup>2</sup>AUM LifeTech, Inc., Philadelphia, PA 19104, USA; <sup>3</sup>Department of Chemistry, McGill University, Montreal, QC H3A 0B8, Canada; <sup>4</sup>Irell and Manella Graduate School of Biological Science, Beckman Institute of City of Hope, Duarte, CA 91010, USA

**Currently, the most effective and durable therapeutic option for HIV-1 infection is combination antiretroviral therapy (cART). Although cART is powerful and can delay viral evolution of drug resistance for decades, it is associated with limitations, including an inability to eradicate the virus and a potential for adverse effects. Therefore, it is imperative to discover new HIV therapeutic modalities. In this study, we designed, characterized, and evaluated the *in vitro* potency of 2'-deoxy-2'-fluoroarabinonucleotide (FANA) modified antisense oligonucleotides (ASOs) targeting highly conserved regions in the HIV-1 genome. Carrier-free cellular internalization of FANA ASOs resulted in strong suppression of HIV-1 replication in HIV-1-infected human primary cells. *In vitro* mechanistic studies suggested that the inhibitory effect of FANA ASOs can be attributed to RNase H1 activation and steric hindrance of dimerization. Using 5'-RACE PCR and sequencing analysis, we confirmed the presence of human RNase H1-mediated target RNA cleavage products in cells treated with FANA ASOs. We observed no overt cytotoxicity or immune responses upon FANA ASO treatment. Together, our results strongly suggest that FANA ASOs hold great promise for antiretroviral therapy. The dual ability of FANA ASOs to target RNA by recruiting RNase H1 and/or sterically blocking RNA dimerization further enhances their therapeutic potential.**

## INTRODUCTION

HIV-1 is the major cause of AIDS. Currently, the most effective and durable therapeutic option for HIV-1 infection is combination antiretroviral therapy (cART), in which three or more antiretroviral drugs with different mechanisms of action are administered.<sup>1</sup> This combination therapy can effectively suppress the level of plasma virus in patients below the limit of detection, and dramatically reduces the mortality of HIV-1-infected patients. However, due to lack of proof-reading ability of the viral reverse transcriptase, HIV-1 has an extremely rapid rate of spontaneous mutation, thus generating enormous genetic diversity. This inherently high frequency of mutation, along with genetic recombination, results in the emergence of drug-resistant variants.<sup>2</sup> Although cART may delay viral evolution of

drug resistance for decades, complete eradication of HIV-1 cannot be achieved using cART alone. Furthermore, lifetime daily medication, which is mandatory for HIV-1-infected patients to maintain viral suppression, increases the patients' risks for a variety of chronic conditions including cardiovascular disorders, diabetes, mitochondrial dysfunction, and cancer.<sup>3</sup> Therefore, ongoing efforts to discover new HIV therapeutic modalities are imperative. The advent of antisense technology to achieve specific silencing of target genes provides a promising opportunity for treating HIV-1 infection.

Antisense oligonucleotides (ASOs)<sup>4</sup> are single-stranded, synthetic nucleic acids that recognize and bind target messenger RNAs (mRNAs) via Watson-Crick base pairing. ASO binding consequently causes degradation of target mRNAs through an RNase H-dependent mechanism or prevents target mRNA translation or splicing through a steric-blocking mechanism. Natural DNA and RNA molecules essentially lack favorable drug-like properties; their instability in biological fluid, poor bioavailability, and potential activation of innate immunity are major obstacles to their use as therapeutics. Thus, introduction of chemical modifications that improve these limitations has become an essential feature in designing ASOs. Chemical modifications are generally introduced to the backbone linkages and/or the 2' position of the sugar moieties of ASOs to provide nuclease stability, enhance targeting potency and pharmacokinetic properties, and reduce the immune response *in vivo*. For example, introduction of a phosphorothioate (PS) backbone, the first chemical modification applied to ASO technology, facilitates oligonucleotide trafficking and cellular uptake.<sup>5</sup> Due to increased hydrophobicity and high affinity for plasma proteins, PS-ASOs, particularly those with sugar 2'-modifications, are able to slowly cross the lipid bilayer to escape endosomes into the cytoplasm and nucleus. However, PS backbone modification alone does not fully protect ASOs from nuclease degradation, and it reduces the binding

Received 5 January 2019; accepted 4 July 2019;  
<https://doi.org/10.1016/j.omtn.2019.07.001>

**Correspondence:** John J. Rossi, Department of Molecular and Cellular Biology, Beckman Research Institute, City of Hope, Monrovia, CA 91016, USA.

**E-mail:** [jrossi@coh.org](mailto:jrossi@coh.org)



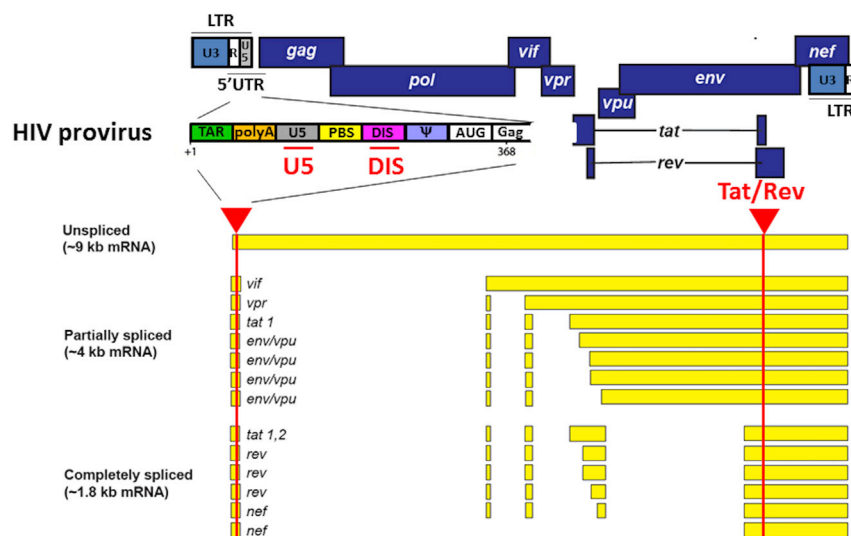


**Figure 1. Schematic Representation of HIV Provirus and Alternative Splicing Patterns**

Arrows indicate target sites of FANA ASOs.

avidity of an oligonucleotide toward its target mRNA. As a result, a variety of sugar modifications, such as 2'-*O*-methoxyethyl (2'-*O*-MOE), 2'-deoxy-2'-fluoro (2'-F), locked nucleic acid (LNA), and 2'-deoxy-2'-fluoro-D-arabinonucleic acid (FANA),<sup>6,7</sup> have been further incorporated to improve nuclease resistance and binding affinity, and reduce immune response. Not surprisingly, most ASOs in pre-clinical development and clinical evaluation contain the PS backbone with extensive sugar modifications.<sup>8-10</sup>

FANA is an oligonucleotide analog comprised of 2'-deoxy-2'-fluoroarabinonucleotides, wherein the fluorine atom is placed on the 2'  $\beta$  position (top-face) of the nucleoside furanose ring. Unlike many 2'-modified analogs that show RNA-like properties, FANA is considered a DNA mimic,<sup>11</sup> forming FANA:RNA hybrids that mimic the structure of the native DNA:RNA hybrid.<sup>12</sup> As a result, FANA, and particularly chimeric FANA-DNA ASOs, are able to elicit RNase H-mediated cleavage of target RNA.<sup>13-15</sup> In addition, 2'-fluoroarabinonucleoside modification significantly enhances chemical and intracellular stability, as well as binding to the target RNA, supporting formation of stable ASO:RNA heteroduplex structures.<sup>16-18</sup> Another interesting feature of FANA was revealed in a recent study by Souleimanian et al.<sup>19</sup> they showed that PS-modified FANA ASOs are compatible with gymnotic delivery in multiple cell lines and are as effective at inhibiting gene expression as corresponding LNA-modified ASOs. More recently, Chorzalska et al.<sup>20</sup> demonstrated that FANA ASOs gymnotically silenced a target gene (Abi-1) with knock-down efficiency greater than 50% in human CD34<sup>+</sup> cells isolated from the bone marrow of healthy donors. Given these attractive features, we reasoned that FANA ASOs against HIV-1 would demonstrate potent and gene-specific antiretroviral activity.

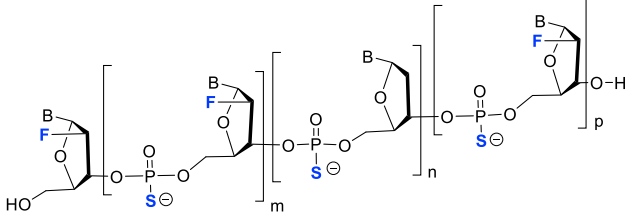
In the present study, we designed, characterized, and evaluated the *in vitro* potency of PS-modified FANA ASOs targeting highly conserved regions in the HIV-1 genome (U5, tat/rev, and the dimerization initiation site [DIS]). Following incubation of FANA ASOs

with primary human peripheral blood mononuclear cells (PBMCs), we observed carrier-free cellular internalization within 3 h. We evaluated the anti-HIV-1 activity of FANA ASOs in PBMCs infected with HIV-1<sub>NL4-3</sub>. HIV-1 expression was effectively suppressed by FANA ASOs with a half maximal inhibitory concentration (IC<sub>50</sub>) of ~200 nM. Our *in vitro* mechanistic studies suggested that the inhibitory effect of the FANA ASOs can likely be attributed to RNase H1 activation (U5 and tat/rev) and steric hindrance (DIS). We confirmed cleavage of RNase H1-mediated target RNA in cells using 5'-RACE PCR and sequencing analysis. The safety of our approach was demonstrated in primary PBMCs from various healthy donors, in which we observed no overt cytotoxicity or immune responses. Taken together, our results support the use of PS-modified FANA ASOs as a potential antiretroviral treatment for HIV-1, which warrants further *in vivo* evaluation.

## RESULTS

### Design of FANA ASOs Targeting the HIV-1 Viral Genome

The HIV-1 genome is approximately 9.7 kb in length and encodes nine major proteins including the structural proteins Gag, Pol (RT, IN, PR), and Env; the regulatory proteins Tat and Rev; and the accessory proteins Vpu, Vpr, Vif, and Nef.<sup>21</sup> A schematic representation of HIV-1 genomic DNA is shown in Figure 1. HIV-1 primary transcripts undergo extensive and complex alternative splicing to produce differently spliced mRNAs that express different viral proteins.<sup>22</sup> Previous studies have demonstrated that all of the HIV-1 encoded genes (i.e., gag, pol, env, tat, rev, vpu, vpr, vif, nef, and the long terminal repeat [LTR]) are susceptible to RNAi-induced gene silencing, suggesting they are potential molecular targets for anti-HIV therapeutics.<sup>23-27</sup> In the present study, we chose tat/rev and the U5 region as ASO targets in the HIV-1 genome, because both sites are highly conserved among the majority of HIV-1 isolates and are present in all un-spliced, partially spliced, and fully spliced HIV-1 RNA, as well as in the viral genomic RNA. Additionally, we designed an ASO against DIS, which is located in the 5' UTR of the viral genomic RNA.<sup>28</sup> DIS is known to be critical for the intermolecular interactions that control dimerization of two copies of identical viral genomic RNA during virion assembly.<sup>29</sup> Mutation or inhibition of DIS severely affects viral infectivity.<sup>29-33</sup> All FANA ASOs used in this study were designed with a PS backbone and a "gapmer" type modification, in which a central DNA region (varying from 1 to 9 nt) was flanked by 2'-fluoroarabinonucleoside residues (Table 1). We also prepared a targeting PS-DNA sequence (DIS-DNA) and a random PS-FANA sequence (SC-FANA) as experimental controls.

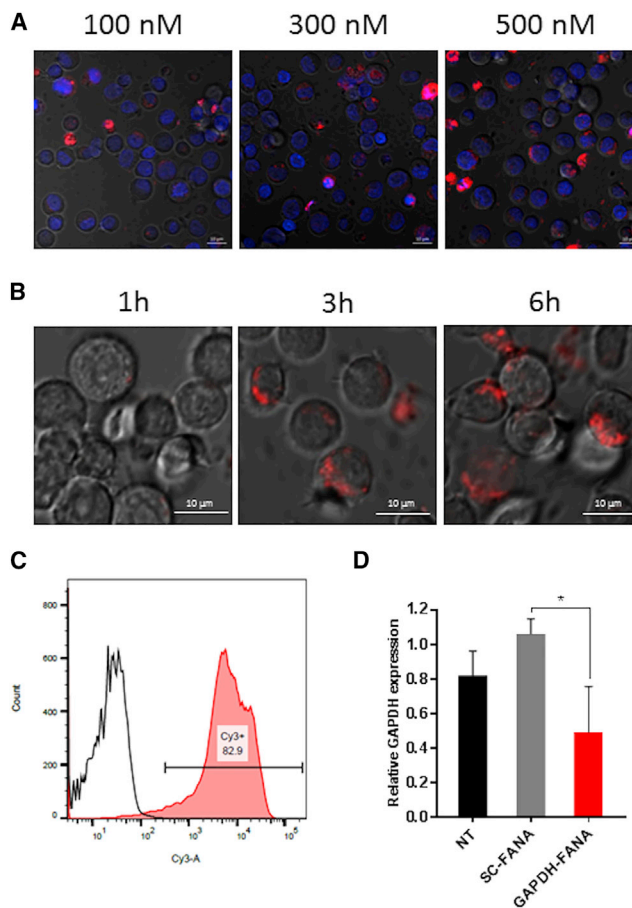
**Table 1. Schematic of FANA-DNA ASO Gapmer and Oligonucleotide Sequences Used in This Study**


ASO	Sequences (5' > 3')	Length	DNA Gap Length
DIS-FANA-G0	UGCCGUGUGCACUUCAGCAA	20	0
DIS-FANA-G1.1	UGCCGUGUGgCACUUCAGCAA	20	1
DIS-FANA-G1.2	UGCCGUGUGcACUUCAGCAA	20	1
DIS-FANA-G2	UGCCGUGUgcACUUCAGCAA	20	2
DIS-FANA-G4	UGCCGUGtgcaCUUCAGCAA	20	4
DIS-FANA-G6	UGCCGUGgtgcacUUCAGCAA	20	6
DIS-FANA-G9	UGCCGtgtgcacttCAGCAA	20	9
DIS-DNA	tgccgtgtgcacttcagca	20	-
tat/rev-FANA	UGAGCtcttcgtcgCUGUCU	20	9
U5-FANA	GUCUGaggatctctAGUAC	21	9
Cy3-FANA	Cy3-UGAGCtcttcgtcgCUGUCU	20	9
Cy3-DIS-FANA-G0	Cy3-UGCCGUGUGCACUUCAGCAA	20	0
Cy3-DIS-DNA	Cy3-tgccgtgtgcacttcagca	20	-
SC-FANA	UGACCCUAtgtgtUCCUAUA	21	6
GAPDH-FANA	CAAGCUtccgttcUCAGCC	20	8
CpG 2395	tcgtcttttcggcgcgccgg	22	-

Lowercase letters represent 2'-deoxyribonucleotides; bold uppercase letters represent 2'-fluoroarabinonucleosides. Backbones are uniformly modified with phosphorothioate (PS) linkages. Cy3 is linked to the 5' end of Cy3-FANA through a PS linkage.

### Carrier-free Cellular Internalization of FANA ASO into Primary PBMCs

It has been reported that intracellular delivery of FANA ASOs in multiple cell lines, including CD34<sup>+</sup> stem cells, can be accomplished in the absence of delivery agents such as carrier vehicles or molecular conjugations.<sup>19,20</sup> Therefore, we first determined whether FANA ASOs could be internalized into PBMCs without the help of delivery agents. We labeled a FANA ASO with Cy3 dye at its 5' end (Cy3-FANA), then incubated it with freshly isolated primary PBMCs and performed real-time, live-cell, z axis confocal microscopy. Carrier-free cellular internalization of Cy3-FANA was dose and time dependent (Figures 2A and 2B). At 4 h post-treatment, the internalized Cy3-FANA was mainly localized in the cytoplasm of cells (Figure S1, z stack). Similarly, dose-dependent cellular internalization was observed in CD8-depleted PBMCs treated with Cy3-FANA or a fully modified FANA ASO with Cy3 dye at its 5' end (Cy3-DIS-FANA-G0). Compared with DIS-DNA, FANA ASOs appeared to be more

**Figure 2. Carrier-free Cellular Internalization Studies of FANA ASO**

(A and B) Real-time live-cell confocal microscopy analysis. (A) PBMCs were incubated with Cy3-FANA at indicated concentrations for 4 h. Representative images were collected using  $\times 40$  magnification. (B) PBMCs were incubated with Cy3-FANA at 100 nM concentration. Images were collected at indicated time points using  $\times 40$  magnification. Red: Cy3-FANA; blue: Hoechst 333342. (C) Cellular uptake level of Cy3-FANA assessed by flow cytometry. PBMCs were incubated with Cy3-FANA at a concentration of 100 nM in complete media for 4 h. After being stained with DAPI, cells were immediately analyzed by flow cytometry. (D) Knockdown of target gene expression (GAPDH) in PBMCs by GAPDH-FANA. Relative GAPDH mRNA expression was detected using quantitative real-time PCR, with HPRT as internal control. An asterisk indicates a significant difference compared with control (\*p < 0.05, two-tailed Student's t test). All experiments were performed in triplicate, and data show mean values from at least three assays, each of which used cells isolated from blood from different donors. NT, non-treated cells. Error bars indicate SD.

effectively internalized into CD8-depleted PBMCs (Figure S2). To quantitate the extent of cellular uptake of Cy3-FANA, we conducted a flow cytometric analysis of PBMCs after 4-h incubation with Cy3-FANA followed by treatment with trypsin to remove unbound ASOs on the cell surface. We observed that 82.9% of cells were Cy3-positive, suggesting that the FANA ASO is internalized within the majority of PBMC subsets (Figure 2C). We observed similar results using a T lymphoblast cell line, CCRF-CEM (Figures S3A and S3B).

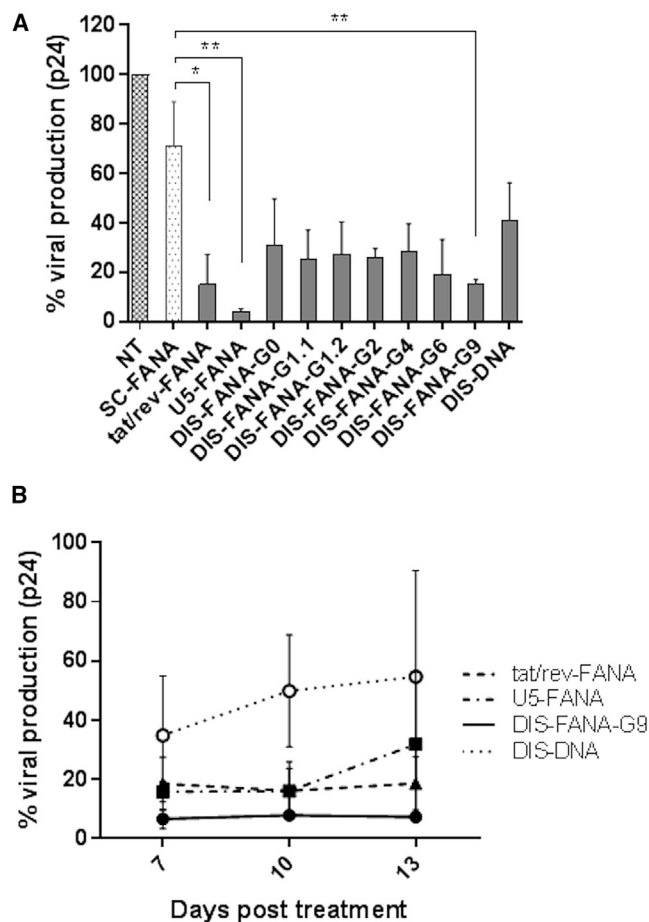


**Figure 3. Inhibition of HIV-1 Replication in HIV-1-Infected Primary CD4<sup>+</sup> T Cells**

(A and B) HIV-1<sub>NL4-3</sub>-infected PBMC-CD4<sup>+</sup> T cells were treated with indicated FANA ASOs at 400 nM (A) or 3 μM (B). Data represent the relative viral production level calculated based on HIV-1 p24 expression. White circles: DIS-DNA; squares: U5-FANA; triangles: tat/rev-FANA; black circles: DIS-FANA-G9. Asterisks indicate significant differences compared with control (SC-FANA) (\*\**p* < 0.01, \**p* < 0.05, two-tailed Student's *t* test). All experiments were performed in triplicate, and data show mean values from at least three assays, each of which used cells isolated from different donors. Error bars indicate SD.

Next, we determined whether the carrier-free, internalized FANA ASO was functional in primary PBMCs. We used a FANA ASO targeting human GAPDH (GAPDH-FANA) as a model molecule and a scrambled FANA ASO (SC-FANA) as a negative control, and incubated each with primary PBMCs at a working concentration of 500 nM. At 3 days post-treatment, to assess knockdown efficiency, we quantified endogenous GAPDH using quantitative real-time PCR (Figure 2D). Compared with treatment with SC-FANA, treatment with GAPDH-FANA resulted in an approximately 50% reduction in GAPDH mRNA expression. These results indicate that FANA ASOs can functionally access target mRNAs upon internalization into PBMCs in the absence of delivery agents.

**Table 2. IC<sub>50</sub> Values of Anti-HIV-1 ASOs**

ASO	HIV-1 Challenge IC <sub>50</sub> (nM) <sup>a</sup>
tat/rev-FANA	169.5 ± 40.8
U5-FANA	176.1 ± 30.9
DIS-FANA-G9	275.6 ± 79.6
DIS-DNA	507.7 ± 140.9

<sup>a</sup>IC<sub>50</sub> values were calculated based on HIV-1 p24 levels in supernatant from HIV-1<sub>NL4-3</sub>-infected PBMCs. Data were collected from three to four independent experiments using primary PBMCs isolated from different healthy donors. Values represent mean ± SD.

### FANA ASOs Targeting the HIV-1 Genome Suppress Viral Replication in HIV-1-Infected Primary CD4<sup>+</sup> T Cells

To evaluate the ability of anti-HIV FANA ASOs to inhibit viral replication, we conducted *in vitro* HIV-1 challenge assays in primary human PBMC-CD4<sup>+</sup> T cells. We challenged freshly isolated PBMC-CD4<sup>+</sup> T cells with HIV-1<sub>NL4-3</sub> at an MOI of 0.01, 4 days prior to treatment with ASOs (400 nM), including FANA ASOs targeting HIV-1 tat/rev, U5, and DIS (G0–G9), a DNA ASO against DIS (DIS-DNA), or a scrambled FANA ASO control (SC-FANA). At 4 days post-treatment, we collected cell-free culture supernatants and examined viral expression levels using HIV-1 p24 ELISA. Compared with non-treated cells, we observed significant suppression of p24 expression (69%–95%) in cells treated with tat/rev-FANA, U5-FANA, and DIS-FANA ASOs (Figure 3A). We also observed ~30% inhibition of viral production in cells treated with SC-FANA when compared with the non-treated cells, which suggests the presence of a nonspecific effect for FANA ASOs.

To evaluate the duration of the anti-HIV effects mediated by selected FANA ASOs, we treated HIV-1<sub>NL4-3</sub>-infected PBMC-CD4<sup>+</sup> cells with indicated FANA ASOs at 3 μM. At 7, 10, and 13 days post-treatment, we collected aliquots of the culture supernatant and again assayed for HIV-1 p24 levels. We observed prolonged inhibition of viral p24 production in anti-HIV-1 FANA ASO-treated cells (Figure 3B). These effects lasted for as long as 13 days after FANA ASO treatment. DIS-DNA showed a moderate anti-HIV effect at day 7 post-treatment, but its inhibitory effect gradually declined over the same 13-day period. Taken together, these results show that FANA ASOs targeting the HIV-1 genome inhibit HIV-1 replication in primary human PBMC-CD4<sup>+</sup> T cells. Tat/rev-FANA and U5-FANA ASOs showed the lowest IC<sub>50</sub> values (170 and 176 nM, respectively), followed by DIS-FANA-G9 (276 nM) and DIS-DNA (508 nM) (Table 2; Figure S4). Notably, we observed no cytotoxicity, as assessed using a 3-(4,5-dimethylthiazol-2-yl)-2,5-diphenyltetrazolium bromide (MTT)-based cell proliferation assay (Figure S5).

### Anti-HIV FANA ASOs Do Not Elicit Any Apparent Immune Response

It is well known that oligonucleotides can potentially activate innate immune response, resulting in production of inflammatory cytokines such as IFN-α and IL-6. Although such immune activation could contribute to the desired antiviral effects, it could also trigger

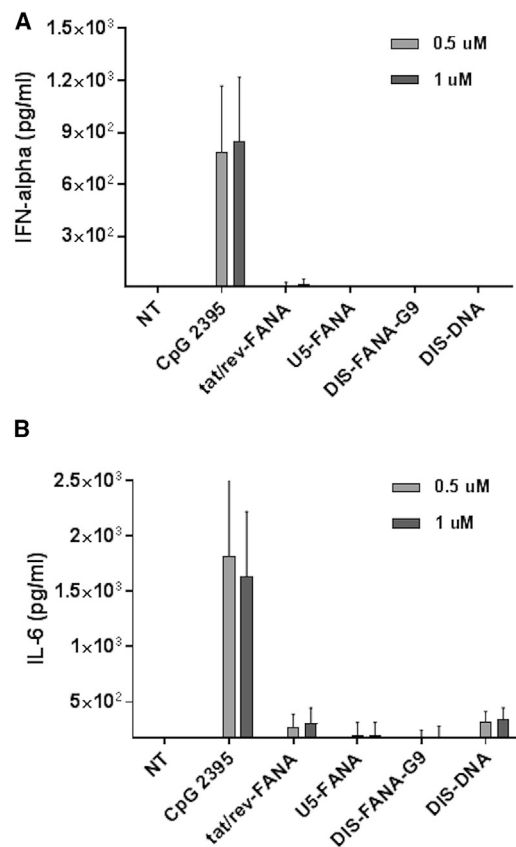


**Figure 4. Immune Response Assays in Human PBMCs**

(A and B) IFN- $\alpha$  (A) and IL-6 (B) expression were measured using ELISA following treatment of primary PBMCs with CpG 2395 (positive control), indicated ASOs, or non-treated control (NT). All experiments were performed in triplicate, and data show mean values from at least four assays, each of which used cells isolated from different donors. Error bars indicate SD.

undesirable cytotoxicity. Therefore, we used ELISA to assess the induction of IFN- $\alpha$  and IL-6 in PBMCs treated with various concentrations of anti-HIV-1 ASOs for 24 h. We used a highly immunostimulatory CpG oligonucleotide (CpG 2395) as a positive control, which is recognized by Toll-like receptor 9 (TLR9) and leads to strong secretion of IFN- $\alpha$  and IL-6.<sup>34</sup> Compared with non-treated cells, we observed a dramatic increase of IFN- $\alpha$  secretion in CpG 2395-treated PBMCs (>500 pg/mL); in contrast, no obvious IFN- $\alpha$  response was detected in the supernatants of any of the anti-HIV-1 ASO-treated PBMCs (Figure 4A). Similarly, we observed dramatically elevated production of IL-6 in CpG 2395-treated PBMCs, but not in anti-HIV FANA ASO-treated PBMCs (Figure 4B). Collectively, these data suggest the tested FANA ASOs do not stimulate an overt immune response.

#### FANA ASOs Induce Specific Target Gene Knockdown through RNase H-Dependent Mechanisms

As described previously, PO- and PS-linked FANA oligonucleotides retain the ability to induce RNase H-mediated degradation of target

RNA. To determine whether the anti-HIV FANA ASOs function through an RNase H-dependent mechanism, we tested their ability to trigger human RNase H1 *in vitro*. We used T7 RNA polymerase to enzymatically synthesize a 5' end <sup>32</sup>P-labeled HIV-1 RNA fragment containing the first 363 nt of HIV-1 genomic RNA (HIV-LTR RNA fragment). This fragment harbors the U5 and DIS target sites at positions 130–150 and 249–267 nt, respectively, but does not contain the tat/rev target site. We performed *in vitro* RNase H1 digestion assays by incubating the HIV-LTR RNA fragment with human RNase H1 at 37°C for 1 h in the absence or presence of unlabeled ASOs, then assessing RNA cleavage. We showed that U5-FANA ASO and DIS-FANA ASOs containing DNA gaps (G1–G9) elicited RNase H1 cleavage of the target RNA (Figure 5A). The products were cleaved primarily at sites complementary to the ASOs. As expected, no cleavage products were detected in the presence of the tat/rev-FANA ASO or in the absence of ASO. We also observed cleavage by DIS-DNA at its complementary site of the target HIV-LTR RNA fragment. We noted differences in cleavage preferences between DIS-FANA ASOs and DIS-DNA. When comparing RNase H1 cleavage activity of the DIS-FANA ASOs containing various sizes of DNA gaps (G1–G9; Table 1), including a fully modified DIS-FANA-G0 (DNA gap = 0), we found that cleavage efficiency was improved when the length of the DNA gap was increased, as previously observed.<sup>15</sup> Consistent with this, DIS-FANA ASO containing nine DNA residues (DIS-FANA-G9) was the most efficient at eliciting RNase H1 cleavage compared with other DIS-FANA ASOs containing shorter DNA gaps (G1–G6). Interestingly, DIS-FANA-G0 and DIS-FANA-G1 also mediated RNase H cleavage, although the cleavage efficiency was dramatically reduced relative to DIS-FANA ASOs containing DNA gaps with  $\geq 2$  nt. Although FANA conforms to the DNA:RNA hybrid structure, a minimal number of DNA residues are necessary to observe substantial RNase H-mediated RNA cleavage. We ascribe this effect to the greater sugar flexibility of DNA versus FANA, which allows for better positioning of the target RNA strand in the RNase H active site, leading to more efficient strand cleavage.<sup>35–37</sup>

Next, to confirm that the FANA ASOs are able to elicit RNase H1 activity in human cells, we demonstrated 5'-rapid amplification of cDNA ends (5'-RACE) PCR. We treated HIV-1-infected PBMCs with U5-FANA ASO, then isolated total RNA and performed 5'-RACE PCR, followed by deep sequencing analysis (Figure 5B). RNA cleavage (ca. 75%) occurred within the residues directly opposite to the cDNA gap of U5-FANA ASO, supporting the notion that target mRNA cleavage in FANA ASO-treated cells is most likely mediated by endogenous RNase H. To further demonstrate activation of RNase H1-mediated cleavage of target RNA, we performed 5'-RACE PCR using HEK293T cells as a model system. We co-transfected HEK293T cells with tat/rev-FANA ASO and a Rev-EGFP fusion construct harboring the tat/rev-FANA ASO target. We used a tat/rev small interfering RNA (siRNA) that shares the same target site with the designed tat/rev-FANA ASO as a positive control. Twenty-four hours after transfection, we isolated total RNA, then performed 5'-RACE to identify the specific cleavage

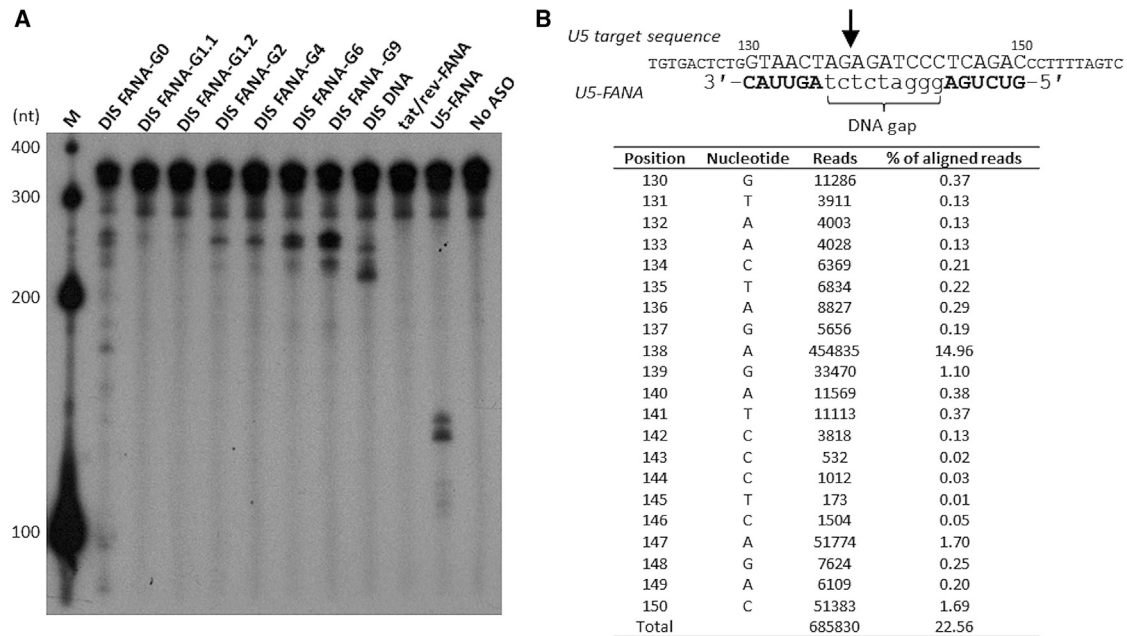


**Figure 5. RNase H-Mediated Cleavage of Target RNA**

(A) A 5'-<sup>32</sup>P-labeled HIV-LTR RNA fragment (363 nt) was incubated with human RNase H1 in the absence or presence of indicated unlabeled ASOs at 37°C for 1 h. The samples were resolved by electrophoresis on a 6% PAGE containing 7 M urea. M, 5'-<sup>32</sup>P-labeled RNA size marker (Century-Plus RNA Markers; Thermo Fisher Scientific). (B) 5'-RACE PCR analysis of viral RNA extracted from PBMCs after treatment with U5-FANA ASO. Nested PCR products were subjected to Illumina high-throughput sequencing analysis. The arrow indicates the position of the major cleavage site in the U5 target RNA.

products in the target transcript. We obtained fragments of the predicted lengths from cells treated with the ASO or with the siRNA (Figure S6). We excised the primary RACE fragment from the ASO-treated sample and inserted it into a pCR2.1 cloning vector using the TA cloning technique. Sequencing of 18 plasmids with the RACE product inserts confirmed that cleavage occurred within the target site complementary to *tat/rev*-FANA ASO. The primary cleavage site was observed between positions 4 and 5 from the 5' end of the ASO, which is different from the RNAi-mediated cleavage site that we previously identified. Of note, this cleavage site was located at a region corresponding to the FANA ASO hybridization site.

#### DIS-FANA ASOs Inhibit Viral RNA Dimerization

Previous studies have shown that ASOs that target the DIS exhibit potent antiviral effects.<sup>30–33</sup> To assess whether the same effect is possible with FANA ASOs, we performed *in vitro* RNA dimerization inhibition assays by incubating the 363-nt HIV-LTR RNA fragment in dimerization buffer containing 5 mM MgCl<sub>2</sub> at 37°C for 30 min with a 1- to 50-fold excess of ASOs. As expected, DIS-FANA-G6 ASO exhibited dramatic reduction in viral RNA dimerization of target RNA, with an efficiency of 26%, 46%, and 68% for ASO ratios of 1:1, 1:10, and 1:50, respectively (Figure 6). In contrast, *tat/rev*-FANA ASO and U5-FANA ASO showed a minimal effect on dimerization, even at higher ASO concentrations (Figure 6; Figure S7). In addition to the bands corresponding to RNA monomer and dimer,

an unknown third band that runs slower than the other two bands was observed when blocking the U5-FANA target region (Figure 6). Given that the interaction between ASO and its target is a dynamic adaption, which may cause structure changes of the highly structured target,<sup>38</sup> we believe that this unknown product may result from the structural changes of the target HIV-LTR RNA fragment. DIS-DNA also decreased RNA dimer formation, but only at 10 and 50 molar excess of the ASO. We also examined the impact of DNA gapmer length on dimerization inhibition. DIS-FANA ASOs with shorter DNA gaps exhibited stronger inhibition of dimerization. The fully 2'-fluoroarabinonucleoside-modified ASO (DIS-FANA-G0; gap = 0) was the most efficient at blocking RNA dimer formation, followed by the ASOs containing a single DNA residue (DIS-FANA-G1; gap = 1). These results provide evidence that extensive 2'-fluoroarabinonucleoside modification enhances the binding of ASOs to target RNA, thereby resulting in strong inhibition of viral RNA dimerization. Taken together, our results suggest that DIS-FANA ASOs can function as a competitive inhibitor of the dimerization process.

#### DISCUSSION

ASOs represent gene-specific therapeutic options for controlling HIV-1 replication via RNase H-dependent or steric blocker-dependent mechanisms. In the present study, we demonstrated potent and durable anti-HIV-1 activity of FANA ASOs targeting the HIV-1 genome in human PBMCs. We targeted three regions of

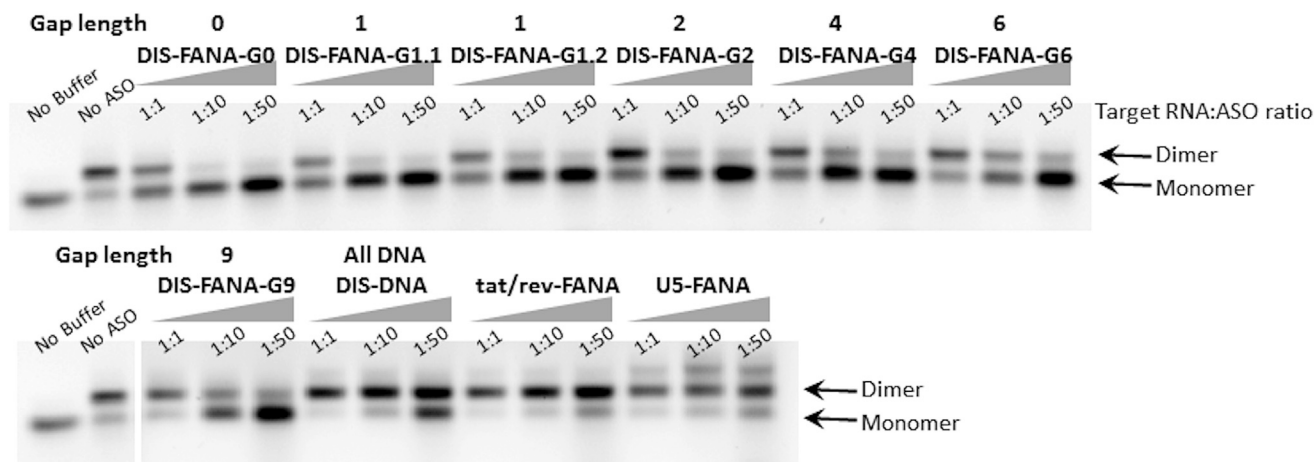


**Figure 6. Inhibition of Viral RNA Dimerization by DIS-FANA ASOs**

HIV-LTR RNA fragment (363 nt) was incubated with human RNase H1 in the absence or presence of indicated ASOs (1:1, 1:10, or 1:50) at 37°C for 30 min under dimerization conditions (i.e., the presence of  $Mg^{2+}$ ). Samples were then resolved on a 1% agarose gel in TBM buffer at 4°C. See also Figure S7.

the HIV-1 genome (*tat/rev*, U5, and DIS) that are highly conserved throughout multiple viral strains, because targeting conserved genomic regions could minimize the emergence of resistant viral variants.

FANA is very unique in that its structure, unlike most other chemical modifications, closely mimics DNA in hybrid ASO:RNA duplexes while retaining high nuclease resistance, target specificity, and high affinity for complementary RNA. The anti-HIV-1 FANA ASOs used in this study are PS-modified FANA-DNA chimeras consisting of a DNA core (or “gap”) flanked by 3′ and 5′ FANA wings. Our results suggest that FANA ASOs are internalized into primary PBMCs by gymnosis, i.e., without any delivery vehicle, where they are mainly located within the cytoplasm, and result in effective target silencing (Figure 2). Souleimanian et al.<sup>19</sup> and Soifer et al.<sup>39</sup> noted that when gymnotic experiments are performed in complete media, high cell confluency may diminish gene silencing activity of ASOs. However, given that PBMCs isolated from healthy donors do not proliferate unless stimulated or activated, we performed all of our experiments in complete media and achieved efficient gymnotic delivery of FANA ASOs into PBMCs.

Treatment of HIV-1-infected human PBMCs with anti-HIV-1 ASOs resulted in strong and prolonged suppression of HIV-1 replication (Figure 3). We also observed non-sequence-specific viral suppression in SC-FANA ASO-treated cells. Studies have suggested that a variety of host proteins and viral proteins, including gp120, gp41, reverse transcriptase, and integrase, are involved in the observed non-sequence-specific, anti-HIV-1 effects of PS-modified oligonucleotides.<sup>40–46</sup> Therefore, the non-sequence-specific inhibition we observed could be explained by PS backbone-mediated interactions between viral proteins and PS-modified oligonucleotides. On the other hand, the catalytic metabolites of FANA ASOs including 2′-deoxy-2′-fluoroarabinnucleosides and their nucleotides reportedly have antiviral effects

against herpes simplex virus (HSV), hepatitis B virus (HBV), and Epstein-Barr virus (EBV).<sup>47–49</sup> To the best of our knowledge, no study has shown anti-HIV-1 activity of 2′-deoxy-2′-fluoroarabinnucleosides and their nucleotides. Although limited, the possibility of anti-HIV-1 effect of these metabolites cannot be excluded. Nevertheless, the antiviral effect of FANA ASOs was more potent than SC-FANA or DIS-DNA ASOs, suggesting that non-sequence-specific effects act synergistically with sequence-specific interactions to block viral replication.

It is important to note again that unlike most chemical modifications, FANA-DNA chimeras exhibit enhanced binding affinity to target RNA while retaining the ability to activate RNase H1. Therefore, we surmise that dual mechanisms of action, RNase H1 activation and steric hindrance, underlie the observed inhibition of viral replication. We observed RNA fragments consistent with RNase H-mediated cleavage of the target viral RNA (Figure 5A). Furthermore, we showed that FANA-DNA ASO gapmers retained the ability to activate human RNase H1 in cells, and high-affinity DIS-FANA ASOs harboring shorter DNA gaps acted as competitive inhibitors of the viral dimerization process, likely by interfering with the kissing-loop interaction between two viral genomic RNAs (Figure 6).<sup>50</sup> These *in vitro* mechanistic studies suggest that depending on the antisense construct (gapmer or fully modified), DIS-FANA ASOs function as activators of RNase H1, as well as competitive inhibitors of the dimerization process.

In summary, we have demonstrated the therapeutic potential of phosphorothioated FANA ASOs for the treatment of HIV-1. The target sequences used in this study are highly conserved among multiple HIV-1 strains, limiting the likelihood of therapeutic escape. Although we tested only the FANA ASOs in subtype B HIV<sub>NL-4-3</sub>, the encouraging results we obtained suggest that FANA ASOs may be applicable to various HIV-1 strains. In addition, ASO therapeutics can be multiplexed to prevent escape by combining multiple ASOs

targeting various viral and cellular mRNAs, or by combining them with other anti-HIV-1 therapy strategies, such as antiretroviral drugs, siRNA, ribozymes, HIV-1 vaccines, and cell-based therapy. Although some major clinical challenges of ASOs remain to be overcome (e.g., *in vivo* delivery), we are encouraged by the recent approvals of several ASOs by regulatory authorities and the entrance of additional candidates with improved chemical modifications into advanced phases of human clinical trials. The encouraging properties we observed for FANA ASOs (self-delivery, no toxicity, sequence specificity, and potency) make them ideal candidates for further studies. The dual ability of FANA ASOs to target RNA by recruiting RNase H1 and/or sterically blocking RNA dimerization further enhances the therapeutic potential of FANA ASOs as anti-HIV agents.

## MATERIALS AND METHODS

### Reagents

ASOs used in this study were designed and synthesized by AUM LifeTech (Philadelphia, PA, USA). Unless otherwise noted, all chemicals were purchased from Sigma-Aldrich (St. Louis, MO, USA), all restriction enzymes were obtained from New England BioLabs (NEB, Ipswich, MA, USA), and all cell culture products were purchased from GIBCO (Thermo Fisher Scientific, Waltham, MA, USA). Sources for the other reagents were: Dynabeads CD8 (Thermo Fisher Scientific); iScript Reverse Transcription Supermix for RT-qPCR (Bio-Rad Laboratories, Hercules, CA, USA); SsoAdvanced SYBR Green Supermix (Bio-Rad Laboratories); RNeasy mini kit (QIAGEN, Germantown, MD, USA); RNase-free DNase Set (QIAGEN, Germantown, MD, USA); QIAquick Gel Purification Kit (QIAGEN, Germantown, MD, USA); Hoechst 33342 (Thermo Fisher Scientific); DAPI (Thermo Fisher Scientific); MEGAscript T7 Transcription Kit (Thermo Fisher Scientific); Bio-Spin 30 Columns (Bio-Rad Laboratories); Alliance HIV-1 P24 antigen ELISA kit (PerkinElmer, Waltham, MA, USA); Human IFN- $\alpha$  ELISA kit (R&D Systems, Minneapolis, MN, USA); IL-6 ELISA kit (Thermo Fisher Scientific); human RNase H1 (Abcam, Cambridge, UK); ZR Small-RNA PAGE Recovery Kit (Zymo Research, Irvine, CA, USA); and STAT-60 (TELETEST, Friendswood, TX, USA). The infectious molecular clone HIV-1<sub>NL4-3</sub> was obtained from the NIH AIDS Reagent Program.

Primers were purchased from Integrated DNA Technologies (IDT, Coralville, IA, USA): GAPDH forward primer: 5'-CAT TGA CCT CAA CTA CAT G-3'; GAPDH reverse primer: 5'-TCT CCA TGG TGA AGA C-3'; HPRT forward primer: 5'-TGA CAC TGG CAA AAC AAT GCA-3'; HPRT reverse primer: 5'-GGT CCT TTT CAC CAG CAA GCT-3'; primers for 5'-RACE PCR: pNL4-3UTR-1: 5'-AGT CGC CCC TCG CCT CTT G-3'; 5'-cDNA primer: 5'-GGA CAC TGA CAT GGA CTG AAG GAG TA-3'; pNL4-3UTR-2: 5'-AGG GAT GGT TGT AGC TGT CCC AGT AT-3'; forward primer for HIV RNA transcript (T7pNL4-3\_FP): 5'-TAA TAC GAC TCA CTA TAG GGT CTC TCT GGT TAG-3' (the T7 promoter is underlined); reverse primer for HIV RNA transcript (pNL4-3-gag\_RP): 5'-GCT TAA TAC CGA CGC TCT C-3'.

### Cell Lines and Cell Culture

Discarded peripheral blood samples from anonymous, healthy, adult donors were obtained from the City of Hope Apheresis Center (Duarte, CA, USA) for primary cell cultures. PBMCs were isolated from whole blood by centrifugation through a Ficoll-Hypaque solution (Histopaque-1077; Sigma-Aldrich). CD8<sup>+</sup> cells (T cytotoxic and suppressor cells) were depleted from the PBMCs using Dynabeads CD8 according to the manufacturer's instructions. CD8<sup>+</sup> T cell-depleted PBMCs were washed twice in PBS and resuspended in culture media (RPMI-1640 with 10% FBS, 1 $\times$  penicillin-streptomycin [PenStrep], and 60 U/mL IL-2). Cells were used immediately or cultured in a humidified 5% CO<sub>2</sub> incubator at 37°C. This project was evaluated by the Institutional Review Board (IRB) of City of Hope and determined not to involve human subjects research per federal regulation 45 CFR 46.102 (d)(f); therefore, we did not need to obtain informed consent or IRB approval (IRB#/REF#: 97071/075546).

### Internalization and Intercellular Localization (Live-Cell Confocal Microscopy)

On the day experiments were performed, freshly isolated human PBMCs were washed twice with pre-warmed PBS and seeded in a polylysine-coated, four-compartment, 35/10-mm plate at 0.5  $\times$  10<sup>6</sup> cells per compartment in 500  $\mu$ L pre-warmed RPMI-1640 medium supplemented with 10% FBS. Cells were incubated for 30–60 min in a humidified 5% CO<sub>2</sub> incubator at 37°C to allow attachment to the dish surface. Cy3-labeled ASOs (100, 300, or 500 nM) were added to the media, and cells were incubated in a 5% CO<sub>2</sub> microscopy incubator at 37°C for 4 h. The cells were stained by treatment with 0.15 mg/mL Hoechst 33342 according to the manufacturer's instructions. The images were collected using a Zeiss LSM 510 Meta Inverted two-photon confocal microscopy system (City of Hope Confocal Microscopy Core, Duarte, CA, USA) underwater immersion at  $\times$ 40 magnification.

### Cellular Uptake Analysis (Flow Cytometry)

Freshly isolated PBMCs were seeded in a 48-well plate at 2  $\times$  10<sup>5</sup> cells/well in 200  $\mu$ L pre-warmed RPMI-1640 medium supplemented with 10% FBS. Cy3-labeled ASOs were added to the cells at a final concentration of 100 nM. After 4-h incubation, cells were washed with PBS and treated with trypsin for 5 min at 37°C. Cells were washed again and stained with DAPI. Cells were immediately analyzed using flow cytometry (BD LSR-Fortessa; City of Hope Analytical Cytometry Core, Duarte, CA, USA). Data were analyzed using FlowJo version 8.8.6 software.

### Target Gene Knockdown (Quantitative Real-Time PCR)

Freshly isolated PBMCs were seeded into a 24-well plate at 5  $\times$  10<sup>5</sup> cells/well in 500  $\mu$ L RPMI-1640 supplemented with 10% FBS and 60 U/mL IL-2. ASOs were added into each well at a final concentration of 0.5  $\mu$ M. After 72-h incubation at 37°C, cells were collected and washed with PBS. Total RNA was isolated using a RNeasy mini kit according to the manufacturer's protocol. During total RNA isolation, residual DNA was digested using the RNase-free DNase Set. cDNA



was obtained from 1 µg of total RNA using iScript Reverse Transcription Supermix. Expression of GAPDH mRNA was analyzed using quantitative real-time PCR using SsoAdvanced SYBR Green Supermix. Primers are described under [Reagents](#). HPRT expression was used for normalization of the qPCR data. We confirmed that no change occurs in HPRT expression upon ASO treatment. Asterisks indicate a significant difference compared with scrambled control (SC-FANA) (\* $p < 0.05$ , two-tailed Student's  $t$  test). All experiments were performed in triplicate, and data show mean values from at least three assays, each of which used cells isolated from blood from different donors.

#### HIV-1 Challenge Assay

Human PBMCs were freshly isolated from healthy donors, and CD8 cells were depleted from the PBMCs using Dynabeads CD8. After culture for 3 days in activated T cell culture medium, cells were washed with pre-warmed PBS and infected with HIV-1<sub>NL4-3</sub> at an MOI of 0.01 for 4 days. The infected cells were gently washed with pre-warmed PBS three times to remove free virus and resuspended with RPMI-1640 medium containing 60 U/mL IL-2. Infected cells and uninfected cells were mixed at a 1:1 ratio, and the mixed cells were seeded in a 48-well plate at  $5 \times 10^5$  cells/well. ASOs were added to the cells at 400 nM. Aliquots of the culture supernatants were collected at various time points, and HIV-1 p24 ELISA was performed. The percent of viral production was calculated using the formula: p24 expression in the samples/p24 expression in the ASO non-treated sample. SC-FANA was used as a negative control.

#### Immune Response Assay

PBMCs were plated in 24-well plates at  $2.5 \times 10^6$  cells/well in 500 µL RPMI-1640 supplemented with 10% FBS on the day of the experiment. Cells were treated with ASOs at indicated concentrations. After 24 h, supernatant from each well was collected, and IFN- $\alpha$  and IL-6 levels were quantified by ELISA using 96-well ELISA plates coated with human IFN- $\alpha$  or IL-6 antibody, respectively. CpG 2395 was used as a positive control.

#### Generation of the HIV-LTR RNA Fragment

A double-stranded DNA template for T7 transcription was directly generated using PCR with pNL4-3 plasmid as a template and primers (described in [Reagents](#)), and the resulting PCR product was recovered using a QIAquick Gel Purification Kit. The HIV-LTR RNA fragment was transcribed from its PCR-generated DNA template using the MEGAscript T7 Transcription Kit in accordance with the manufacturer's instructions. The reactions were incubated at 37°C for 8 h and subsequently purified using Bio-Spin 30 Columns after phenol extraction and ethanol precipitation. The sample was resolved on a 5% polyacrylamide gel containing 7 M urea, and the full-length HIV-LTR RNA fragment was recovered from the gel.

#### Human RNase H1 Cleavage Assay

The HIV-LTR RNA fragment was incubated in CIP Buffer supplemented with CIP (alkaline phosphatase, calf intestinal; NEB, Ipswich, MA, USA). The mixture was incubated at 37°C for 1 h. After phenol-

chloroform extraction and ethanol precipitation, the RNA pellet was resuspended in water. The dephosphorylated HIV-LTR RNA fragment was incubated at 95°C for 3 min, then chilled on ice. RNA samples were incubated in polynucleotide kinase (PNK) buffer supplemented with T4 DNA kinase,  $\gamma$ -ATP, and RNase inhibitor at 37°C for 30 min. RNA labeled with  $^{32}$ P at the 5' end was purified using Bio-Spin 30 Columns. The sample was loaded onto a 6% polyacrylamide sequencing gel containing 7 M urea. The labeled RNA was recovered from the gel using a ZR Small-RNA PAGE Recovery Kit. 5'- $^{32}$ P-labeled RNA (5 pmol) was mixed with 30 pmol ASO in annealing buffer (1 $\times$ : 10 mM Tris [pH 7.5], 50 mM NaCl, 1 mM EDTA). The sample was denatured at 90°C for 3 min and slowly cooled to room temperature. To initiate the cleavage reaction, we added human RNase H1 (0.07 µg) to the RNA sample in reaction buffer (60 mM Tris-HCl [pH 7.8], 60 mM KCl, 2.5 mM MgCl<sub>2</sub>, and 2 mM DTT) supplemented with 1 µL RNasin Plus RNase Inhibitor (Promega, Madison, WI, USA). The reaction mixture was incubated at 37°C for 1 h. The reaction was quenched with an equal volume of denaturing loading buffer (98% deionized formamide, 10 mM EDTA, 1 mg/mL bromophenol blue [BPB], and 1 mg/mL xylene cyanole [XC]). The sample was then heated at 90°C for 5 min to deactivate the enzyme and denature the strands. The sample was resolved using electrophoresis on a 6% polyacrylamide gel containing 7 M urea. Following electrophoresis, the gel was exposed to a Phosphor image screen, and radioactivity was quantified using a Typhoon scanner.

#### 5'-RACE Assay to Detect Target RNA Cleavage

Total RNA from PBMCs treated with 1.6 µM FANA-U5 ASO was isolated using STAT-60 in accordance with the manufacturer's protocol. Residual DNA was digested using TURBO DNA-free kit in accordance with the manufacturer's instructions (Thermo Fisher Scientific). Subsequently, total RNA (10 µg) was ligated to a GeneRacer adapter (5'-CGA CTG GAG CAC GAG GAC ACT GAC ATG GAC TGA AGG AGT AGA AA-3'; Thermo Fisher Scientific) without prior treatment. Ligated RNA was reverse transcribed using a gene-specific primer 1; to detect cleavage products, we performed nested PCR using primers complementary to the RNA adaptor (and gene-specific primer 2; primers are described in [Reagents](#)). The PCR product was subjected to Illumina high-throughput sequencing analysis. Sample preparation and sequencing were performed by the City of Hope DNA Sequencing Core and Integrative Genomics Core (City of Hope, Duarte, CA, USA).

#### Dimerization Inhibition Assay

The HIV-LTR RNA fragment (10 pmol) and ASOs were mixed at various ratios (1:1–50) in RNase-free water. The mixtures were denatured at 95°C for 3 min and then placed on ice. The RNA mixture was incubated in dimerization buffer (50 mM sodium cacodylate [pH 7.5], 250 mM KCl, 5 mM MgCl<sub>2</sub>) supplemented with 1 µL RNasin Plus RNase Inhibitor at 37°C. After 30 min, the reaction was stopped by adding 2 µL loading dye (4 $\times$ , 10 mM Tris-HCl [pH 7.5]; 1 mM EDTA, 0.1% BPB, 0.1% XC, 0.1% orange G, 40% glycerol). Samples were then resolved using electrophoresis on a 1% agarose gel in

TBM buffer (89 mM Tris-Borate [pH 8.3], 0.2 mM MgCl<sub>2</sub>) at 4°C and visualized using ethidium bromide staining.

## SUPPLEMENTAL INFORMATION

Supplemental Information can be found online at <https://doi.org/10.1016/j.omtn.2019.07.001>.

## AUTHOR CONTRIBUTIONS

Conceptualization, M.T., J.Z., V.A., M.J.D., and J.J.R.; Methodology, M.T., H.L., and J.Z.; Investigation, M.T., H.L., J.Z., and P.C.; Writing – Original Draft, M.T.; Writing – Review & Editing, M.T., J.Z., M.J.D., and J.J.R.; Funding Acquisition, J.J.R.; Resources, V.A.; Supervision, M.J.D. and J.J.R. All authors read and approved the final article.

## CONFLICTS OF INTEREST

The authors declare no competing interests.

## ACKNOWLEDGMENTS

We thank Dr. Piotr Swiderski for providing CPG2395. We thank the City of Hope DNA Sequencing Core and Integrative Genomics Core facility (Shu Tao and Jinhui Wang) for DNA sequencing, Solexa deep sequencing, and data processing. We thank the City of Hope Analytical Cytometry Core (Lucy Brown) for help and technical support of flow cytometry analysis. We thank Dr. Brian Armstrong from the City of Hope Light Microscopy Core for technical support of confocal microscopy imaging. We thank Dr. Sarah T. Wilkinson (Scientific Writer, City of Hope) for helpful advice in scientific writing. This work was supported by the NIH (grants R01AI29329, R01AI42552, and R01HL07470 to J.J.R., as well as grant P30CA033572 for City of Hope Core Facility support). Funding for the open access charge was provided by the NIH. The content is solely the responsibility of the authors and does not necessarily represent the official views of the NIH.

## REFERENCES

- Ghosh, R.K., Ghosh, S.M., and Chawla, S. (2011). Recent advances in antiretroviral drugs. *Expert Opin. Pharmacother.* *12*, 31–46.
- Iyidogan, P., and Anderson, K.S. (2014). Current perspectives on HIV-1 antiretroviral drug resistance. *Viruses* *6*, 4095–4139.
- Reust, C.E. (2011). Common adverse effects of antiretroviral therapy for HIV disease. *Am. Fam. Physician* *83*, 1443–1451.
- Bennett, C.F., and Swayze, E.E. (2010). RNA targeting therapeutics: molecular mechanisms of antisense oligonucleotides as a therapeutic platform. *Annu. Rev. Pharmacol. Toxicol.* *50*, 259–293.
- Eckstein, F. (2014). Phosphorothioates, essential components of therapeutic oligonucleotides. *Nucleic Acid Ther.* *24*, 374–387.
- Fortin, M., D'Anjou, H., Higgins, M.E., Gougeon, J., Aubé, P., Moktefi, K., Mouissi, S., Séguin, S., Séguin, R., Renzi, P.M., et al. (2009). A multi-target antisense approach against PDE4 and PDE7 reduces smoke-induced lung inflammation in mice. *Respir. Res.* *10*, 39.
- Kalota, A., Karabon, L., Swider, C.R., Viazovkina, E., Elzagheid, M., Damha, M.J., and Gewirtz, A.M. (2006). 2'-deoxy-2'-fluoro-β-D-arabinonucleic acid (2'F-ANA) modified oligonucleotides (ON) effect highly efficient, and persistent, gene silencing. *Nucleic Acids Res.* *34*, 451–461.
- Khvorova, A., and Watts, J.K. (2017). The chemical evolution of oligonucleotide therapies of clinical utility. *Nat. Biotechnol.* *35*, 238–248.
- Stein, C.A., and Castanotto, D. (2017). FDA-approved oligonucleotide therapies in 2017. *Mol. Ther.* *25*, 1069–1075.
- Shen, X., and Corey, D.R. (2018). Chemistry, mechanism and clinical status of antisense oligonucleotides and duplex RNAs. *Nucleic Acids Res.* *46*, 1584–1600.
- Martín-Pintado, N., Yahyaee-Anzahae, M., Campos-Olivas, R., Noronha, A.M., Wilds, C.J., Damha, M.J., and González, C. (2012). The solution structure of double helical arabino nucleic acids (ANA and 2'F-ANA): effect of arabinoses in duplex-hairpin interconversion. *Nucleic Acids Res.* *40*, 9329–9339.
- Denisov, A.Y., Noronha, A.M., Wilds, C.J., Trempe, J.F., Pon, R.T., Gehring, K., and Damha, M.J. (2001). Solution structure of an arabinonucleic acid (ANA)/RNA duplex in a chimeric hairpin: comparison with 2'-fluoro-ANA/RNA and DNA/RNA hybrids. *Nucleic Acids Res.* *29*, 4284–4293.
- Damha, M.J., Wilds, C.J., Noronha, A., Brukner, I., Borkow, G., and Parniak, M.A. (1998). Hybrids of RNA and arabinonucleic acids (ANA and 2'F-ANA) are substrates of ribonuclease H. *J. Am. Chem. Soc.* *120*, 12976–12977.
- Min, K.L., Viazovkina, E., Galarneau, A., Parniak, M.A., and Damha, M.J. (2002). Oligonucleotides comprised of alternating 2'-deoxy-2'-fluoro-β-D-arabinonucleosides and D-2'-deoxyribonucleosides (2'F-ANA/DNA 'altimers') induce efficient RNA cleavage mediated by RNase H. *Bioorg. Med. Chem. Lett.* *12*, 2651–2654.
- Lok, C.N., Viazovkina, E., Min, K.L., Nagy, E., Wilds, C.J., Damha, M.J., and Parniak, M.A. (2002). Potent gene-specific inhibitory properties of mixed-backbone antisense oligonucleotides comprised of 2'-deoxy-2'-fluoro-D-arabinose and 2'-deoxyribose nucleotides. *Biochemistry* *41*, 3457–3467.
- Damha, M.J., Noronha, A.M., Wilds, C.J., Trempe, J.F., Denisov, A., Pon, R.T., and Gehring, K. (2001). Properties of arabinonucleic acids (ANA & 2F-ANA): implications for the design of antisense therapeutics that invoke RNase H cleavage of RNA. *Nucleosides Nucleotides Nucleic Acids* *20*, 429–440.
- Ferrari, N., Bergeron, D., Tedeschi, A.L., Mangos, M.M., Paquet, L., Renzi, P.M., and Damha, M.J. (2006). Characterization of antisense oligonucleotides comprising 2'-deoxy-2'-fluoro-β-D-arabinonucleic acid (FANA): specificity, potency, and duration of activity. *Ann. N Y Acad. Sci.* *1082*, 91–102.
- Watts, J.K., Katolik, A., Viladoms, J., and Damha, M.J. (2009). Studies on the hydrolytic stability of 2'-fluoroarabinonucleic acid (2'F-ANA). *Org. Biomol. Chem.* *7*, 1904–1910.
- Souleimanian, N., Deleavey, G.F., Soifer, H., Wang, S., Tiemann, K., Damha, M.J., and Stein, C.A. (2012). Antisense 2β-deoxy, 2'-fluoroarabino nucleic acids (2'F-ANAs) oligonucleotides: in vitro gymnotic silencers of gene expression whose potency is enhanced by fatty acids. *Mol. Ther. Nucleic Acids* *1*, e43.
- Chorzalska, A., Morgan, J., Ahsan, N., Treaba, D.O., Olszewski, A.J., Petersen, M., Kingston, N., Cheng, Y., Lombardo, K., Schori, C., et al. (2018). Bone marrow-specific loss of *AB11* induces myeloproliferative neoplasm with features resembling human myelofibrosis. *Blood* *132*, 2053–2066.
- Sundquist, W.I., and Kräusslich, H.G. (2012). HIV-1 assembly, budding, and maturation. *Cold Spring Harb. Perspect. Med.* *2*, a006924.
- Stoltzfus, C.M. (2009). Chapter 1. Regulation of HIV-1 alternative RNA splicing and its role in virus replication. *Adv. Virus Res.* *74*, 1–40.
- Zhou, J., Swiderski, P., Li, H., Zhang, J., Neff, C.P., Akkina, R., and Rossi, J.J. (2009). Selection, characterization and application of new RNA HIV gp 120 aptamers for facile delivery of Dicer substrate siRNAs into HIV infected cells. *Nucleic Acids Res.* *37*, 3094–3109.
- Neff, C.P., Zhou, J., Remling, L., Kuruvilla, J., Zhang, J., Li, H., Smith, D.D., Swiderski, P., Rossi, J.J., and Akkina, R. (2011). An aptamer-siRNA chimera suppresses HIV-1 viral loads and protects from helper CD4(+) T cell decline in humanized mice. *Sci. Transl. Med.* *3*, 66ra6.
- Zhou, J., Neff, C.P., Swiderski, P., Li, H., Smith, D.D., Aboellail, T., Remling-Mulder, L., Akkina, R., and Rossi, J.J. (2013). Functional in vivo delivery of multiplexed anti-HIV-1 siRNAs via a chemically synthesized aptamer with a sticky bridge. *Mol. Ther.* *21*, 192–200.
- Zhou, J., Satheesan, S., Li, H., Weinberg, M.S., Morris, K.V., Burnett, J.C., and Rossi, J.J. (2015). Cell-specific RNA aptamer against human CCR5 specifically targets HIV-1 susceptible cells and inhibits HIV-1 infectivity. *Chem. Biol.* *22*, 379–390.

27. Zhou, J., and Rossi, J.J. (2011). Current progress in the development of RNAi-based therapeutics for HIV-1. *Gene Ther.* *18*, 1134–1138.
28. Berkhout, B., and van Wamel, J.L. (2000). The leader of the HIV-1 RNA genome forms a compactly folded tertiary structure. *RNA* *6*, 282–295.
29. van Bel, N., Das, A.T., Cornelissen, M., Abbink, T.E., and Berkhout, B. (2014). A short sequence motif in the 5' leader of the HIV-1 genome modulates extended RNA dimer formation and virus replication. *J. Biol. Chem.* *289*, 35061–35074.
30. Skripkin, E., Paillart, J.C., Marquet, R., Blumenfeld, M., Ehresmann, B., and Ehresmann, C. (1996). Mechanisms of inhibition of in vitro dimerization of HIV type I RNA by sense and antisense oligonucleotides. *J. Biol. Chem.* *271*, 28812–28817.
31. Elmén, J., Zhang, H.Y., Zuber, B., Ljungberg, K., Wahren, B., Wahlestedt, C., and Liang, Z. (2004). Locked nucleic acid containing antisense oligonucleotides enhance inhibition of HIV-1 genome dimerization and inhibit virus replication. *FEBS Lett.* *578*, 285–290.
32. Parkash, B., Ranjan, A., Tiwari, V., Gupta, S.K., Kaur, N., and Tandon, V. (2012). Inhibition of 5'-UTR RNA conformational switching in HIV-1 using antisense PNAs. *PLoS ONE* *7*, e49310.
33. Reyes-Darias, J.A., Sánchez-Luque, F.J., and Berzal-Herranz, A. (2012). HIV RNA dimerisation interference by antisense oligonucleotides targeted to the 5' UTR structural elements. *Virus Res.* *169*, 63–71.
34. Vollmer, J., Weeratna, R., Payette, P., Jurk, M., Schetter, C., Laucht, M., Wader, T., Thuk, S., Liu, M., Davis, H.L., and Krieg, A.M. (2004). Characterization of three CpG oligodeoxynucleotide classes with distinct immunostimulatory activities. *Eur. J. Immunol.* *34*, 251–262.
35. Nielsen, J.T., Stein, P.C., and Petersen, M. (2003). NMR structure of an alpha-L-LNA:RNA hybrid: structural implications for RNase H recognition. *Nucleic Acids Res.* *31*, 5858–5867.
36. Mangos, M.M., Min, K.L., Viazovkina, E., Galarneau, A., Elzagheid, M.I., Parniak, M.A., and Damha, M.J. (2003). Efficient RNase H-directed cleavage of RNA promoted by antisense DNA or 2'-F-ANA constructs containing acyclic nucleotide inserts. *J. Am. Chem. Soc.* *125*, 654–661.
37. Lima, W.F., Rose, J.B., Nichols, J.G., Wu, H., Migawa, M.T., Wyrzykiewicz, T.K., Vasquez, G., Swayze, E.E., and Crooke, S.T. (2007). The positional influence of the helical geometry of the heteroduplex substrate on human RNase H1 catalysis. *Mol. Pharmacol.* *71*, 73–82.
38. Dubois, N., Marquet, R., Paillart, J.C., and Bernacchi, S. (2018). Retroviral RNA dimerization: from structure to functions. *Front. Microbiol.* *9*, 527.
39. Soifer, H.S., Koch, T., Lai, J., Hansen, B., Hoeg, A., Oerum, H., and Stein, C.A. (2012). Silencing of gene expression by gymnotic delivery of antisense oligonucleotides. *Methods Mol. Biol.* *815*, 333–346.
40. Stein, C.A., Matsukura, M., Subasinghe, C., Broder, S., and Cohen, J.S. (1989). Phosphorothioate oligodeoxynucleotides are potent sequence nonspecific inhibitors of de novo infection by HIV. *AIDS Res. Hum. Retroviruses* *5*, 639–646.
41. Stein, C.A., Neckers, L.M., Nair, B.C., Mumbauer, S., Hoke, G., and Pal, R. (1991). Phosphorothioate oligodeoxycytidine interferes with binding of HIV-1 gp120 to CD4. *J. Acquir. Immune Defic. Syndr.* *4*, 686–693.
42. Wyatt, J.R., Vickers, T.A., Roberson, J.L., Buckheit, R.W., Jr., Klimkait, T., DeBaets, E., Davis, P.W., Rayner, B., Imbach, J.L., and Ecker, D.J. (1994). Combinatorially selected guanosine-quartet structure is a potent inhibitor of human immunodeficiency virus envelope-mediated cell fusion. *Proc. Natl. Acad. Sci. USA* *91*, 1356–1360.
43. Vaillant, A., Juteau, J.M., Lu, H., Liu, S., Lackman-Smith, C., Ptak, R., and Jiang, S. (2006). Phosphorothioate oligonucleotides inhibit human immunodeficiency virus type 1 fusion by blocking gp41 core formation. *Antimicrob. Agents Chemother.* *50*, 1393–1401.
44. Marshall, W.S., Beaton, G., Stein, C.A., Matsukura, M., and Caruthers, M.H. (1992). Inhibition of human immunodeficiency virus activity by phosphorothioate oligodeoxycytidine. *Proc. Natl. Acad. Sci. USA* *89*, 6265–6269.
45. Stein, C.A., Cleary, A.M., Yakubov, L., and Lederman, S. (1993). Phosphorothioate oligodeoxynucleotides bind to the third variable loop domain (v3) of human immunodeficiency virus type 1 gp120. *Antisense Res. Dev.* *3*, 19–31.
46. Jing, N., Marchand, C., Liu, J., Mitra, R., Hogan, M.E., and Pommier, Y. (2000). Mechanism of inhibition of HIV-1 integrase by G-tetrad-forming oligonucleotides in vitro. *J. Biol. Chem.* *275*, 21460–21467.
47. Watanabe, K.A., Reichman, U., Hirota, K., Lopez, C., and Fox, J.J. (1979). Nucleosides. 110. Synthesis and antiherpes virus activity of some 2'-fluoro-2'-deoxyarabino-furanosylpyrimidine nucleosides. *J. Med. Chem.* *22*, 21–24.
48. Kong, X.B., Scheck, A.C., Price, R.W., Vidal, P.M., Fanucchi, M.P., Watanabe, K.A., Fox, J.J., and Chou, T.C. (1988). Incorporation and metabolism of 2'-fluoro-5-substituted arabinosyl pyrimidines and their selective inhibition of viral DNA synthesis in herpes simplex virus type 1 (HSV-1)-infected and mock-infected Vero cells. *Antiviral Res.* *10*, 153–166.
49. Chu, C.K., Ma, T., Shanmuganathan, K., Wang, C., Xiang, Y., Pai, S.B., Yao, G.Q., Sommadossi, J.P., and Cheng, Y.C. (1995). Use of 2'-fluoro-5-methyl-beta-L-arabino-furanosyluracil as a novel antiviral agent for hepatitis B virus and Epstein-Barr virus. *Antimicrob. Agents Chemother.* *39*, 979–981.
50. Paillart, J.C., Skripkin, E., Ehresmann, B., Ehresmann, C., and Marquet, R. (1996). A loop-loop "kissing" complex is the essential part of the dimer linkage of genomic HIV-1 RNA. *Proc. Natl. Acad. Sci. USA* *93*, 5572–5577.

**OMTN, Volume 17**

**Supplemental Information**

**Dual Mechanisms of Action of Self-Delivering,  
Anti-HIV-1 FANA Oligonucleotides as a Potential  
New Approach to HIV Therapy**

**Mayumi Takahashi, Haitang Li, Jiehua Zhou, Pritsana Chomchan, Veenu  
Aishwarya, Masad J. Damha, and John J. Rossi**

## **Supplemental Information**

### **Dual Mechanisms of Action of Self-Delivering Anti-HIV-1 FANA Oligonucleotides as a Potential New Approach to HIV Therapy**

Mayumi Takahashi<sup>1</sup>, Haitang Li<sup>1</sup>, Jiehua Zhou<sup>1</sup>, Pritsana Chomchan<sup>1</sup>, Veenu Aishwarya<sup>2</sup>, Masad J. Damha<sup>3</sup> and John J. Rossi<sup>1,4</sup>

<sup>1</sup> Department of Molecular and Cellular Biology, Beckman Research Institute, City of Hope, Monrovia, CA, USA 91016

<sup>2</sup> AUM LifeTech, Inc., Philadelphia, PA, USA 19104

<sup>3</sup> Department of Chemistry, McGill University, Montreal, QC, Canada H3A 0B8

<sup>4</sup> Irell and Manella Graduate School of Biological Science, Beckman Institute of City of Hope, Duarte, CA, 91010

## **Materials and Methods**

### **Cell lines and cell culture**

All cells were cultured in a humidified 5% CO<sub>2</sub> incubator at 37°C. HEK293T cells were purchased from ATCC and cultured in 90% DMEM supplemented with 10% fetal bovine serum. HEK293T cells are an adherent cell line and were split 1:10 or 1:5 twice per week upon reaching confluence by washing with PBS and detaching cells using Cell stripper (Cellgro, Mediatech Inc) in order to minimize the damage to the cellular surface receptors. The cells were stained with Trypan Blue to detect viability; >95% live cells were used for seeding. Cells were carried for no more than 15 passages. CCRF-CEM cells were purchased from ATCC and cultured in RPMI-1640 supplemented with 10% fetal bovine serum (FBS). The CCRF-CEM cell line is a suspension cell line and was split 1:10 once per week upon reaching confluence.

### **Internalization and intercellular localization studies (live-cell confocal microscopy) (Figure S1)**

On the day of experiments, PBMCs were washed twice with pre-warmed PBS and seed in a polylysine-coated 4-compartment 35/10-mm plate with seeding at  $0.5 \times 10^6$  cells in 500  $\mu$ L pre-warmed RPMI-1640 medium supplemented with 10% FBS. Cells were incubated for 30-60 min in a humidified 5% CO<sub>2</sub> incubator at 37°C for attaching on the dish surface. Cy3-labeled Cy3-FANA ASOs (100 nM) were added to media and incubated on a 5% CO<sub>2</sub> microscopy incubator at 37°C for 4 h. The cells were stained by treatment with 0.15 mg/ml Hoechst 33342 (Thermo Fisher Scientific, Waltham, MA) according to the manufacturer's instructions. The z-stack images were collected with the step size of 1  $\mu$ m using a Zeiss LSM 510 Meta Inverted two-photon confocal microscopy system (City of Hope Confocal Microscopy Core, Duarte, CA) under water immersion at 40 $\times$  magnification.

### **Internalization studies of CD8-depleted PBMCs (live-cell confocal microscopy) (Figure S2)**

On the day of experiments, human PBMCs were freshly isolated from healthy donors and CD8 cells were depleted from the PBMCs using Dynabeads CD8 (Thermo Fisher Scientific) as described in the main text. CD8-depleted PBMCs were washed twice with pre-warmed PBS and seed in a polylysine-coated 4-compartment 35/10-mm plate with seeding at  $0.5 \times 10^6$  cells in 500  $\mu$ L pre-warmed RPMI-1640 medium supplemented with 10% FBS. Cells were incubated for 30-60 min in a humidified 5% CO<sub>2</sub> incubator at 37°C for attaching on the dish surface. Cy3-labeled ASOs (100 nM, 300 nM, 500 nM) were added to media and incubated on a 5% CO<sub>2</sub> microscopy incubator at 37°C for 4 h. The cells were stained by treatment with 0.15 mg/ml Hoechst 33342 (Thermo Fisher Scientific, Waltham, MA) according to the manufacturer's instructions. The images were collected as described in the main text.

### **Internalization and intercellular localization studies of CCRF-CEM cells (live-cell confocal microscopy) (Figure S3A)**

On the day of experiments, PBMCs were washed twice with pre-warmed PBS and seed in a polylysine-coated 4-compartment 35/10-mm plate with seeding at  $2.5 \times 10^5$  cells in 500  $\mu$ L pre-warmed RPMI-1640 medium supplemented with 10% FBS. Cells were incubated for 30-60 min in a humidified 5% CO<sub>2</sub> incubator at 37°C for attaching on the dish surface. Cy3-FANA ASOs (50 nM, 100 nM, 300 nM) were added to media and incubated on a 5% CO<sub>2</sub> microscopy incubator at 37°C for 4 h. The cells were stained by treatment with 0.15 mg/ml Hoechst 33342 (Thermo Fisher Scientific, Waltham, MA) according to the manufacturer's instructions. The images were collected as described in the main text.

### **Cellular uptake analysis of CCRF-CEM cells (flow cytometry) (Figure S3B)**

CCRF-CEM cells were seeded in a 48-well plate at  $1 \times 10^5$  cells per well in 200  $\mu$ L pre-warmed RPMI-1640 medium supplemented with 10% FBS. Cy3-FANA was added to the cells at a final concentration of 100 nM. After 4 h incubation, cells were washed with PBS and treated with trypsin for 5 min at 37°C. Cells were washed again and stained with DAPI (Thermo Fisher Scientific, Waltham, MA). Cells were immediately analyzed using flow cytometry as described in the main text.

### **HIV-1 challenge assay (dose-response study) (Figure S4)**

Human PBMCs were freshly isolated from healthy donors and CD8 cells were depleted from the PBMCs using Dynabeads CD8 (Thermo Fisher Scientific) as described in the main text. After cultured for 3 days in the activated T-cell culture medium, cells were washed with pre-warmed PBS and infected with HIV-1<sub>NL4-3</sub> at MOI of 0.01 for four days. The infected cells were gently washed with pre-warmed PBS three times to remove free virus and resuspended with RPMI-1640 medium containing 60 units/mL IL-2. Infected cells and uninfected cells were mixed at 1:1 ratio and the mixed cells were seeded in a 48-well plate at  $5 \times 10^5$  cells per well. ASOs were added to the cells at final concentrations of 100 nM, 200 nM, 400 nM, 800 nM or 1600 nM. Culture supernatants were collected at 7-day post-treatment for HIV-1 p24 ELISA (PerkinElmer, Waltham, MA). The % viral production was calculated by the formula: p24 expression amount in the samples/p24 expression amount in the ASO non-treated sample (NT).

### **Cytotoxicity assay (Figure S5)**

Human PBMCs were freshly isolated from healthy donors and CD8 cells were depleted from the PBMCs using Dynabeads CD8 (Thermo Fisher Scientific) as described in the main text. Cells were infected with HIV-1<sub>NL4-3</sub> as described above. Infected cells and uninfected cells were mixed at a 1:1 ratio and the mixed cells were seeded in a 96-well plate at  $2 \times 10^5$  cells per well. ASOs were added to the cells at a final concentration of 3  $\mu$ M for 10 days. Cytotoxicity was measured using CellTiter 96<sup>®</sup> Aqueous One Solution Cell Proliferation Assay System (Promega, Madison, WI) according to the manufacturer's protocol.

### **5'-RACE assays to detect target RNA cleavage in HEK293T cells (Figure S6)**

Twenty-four h before transfection, HEK293T cells were seeded in 6-well plates at  $3 \times 10^5$  cells per well in 1 mL pre-warmed DMEM medium supplemented with 10% FBS. Tat/rev siRNA (sense: 5'-GCG GAG ACA GCG ACG AAG AGC UCA UCA-3'; antisense: 5'-UGA UGA GCU CUU CGU CGC UGU CUC CGC dTdT-3') or tat/rev-FANA (final concentration of each at 50 nM) was co-transfected with a Rev-EGFP fusion construct harboring the tat/rev target using Lipofectamine2000 (Thermo Fisher Scientific, Waltham, MA) according to the manufacturer's protocol. After a 48-h incubation, total RNA was isolated from cells using STAT-60 (TEL-TEST, Friendswood, TX). Residual DNA was digested using the DNA-free kit (Thermo Fisher Scientific, Waltham, MA) per the manufacturer's instructions. Subsequently, total RNA (10  $\mu$ g) was ligated to a GeneRacer adaptor (5'-CGA CTG GAG CAC GAG GAC ACT GAC ATG GAC TGA AGG AGT AGA AA-3', Thermo Fisher Scientific, Waltham, MA) without prior treatment. Ligated RNA was reverse transcribed using a gene-specific primer 1 (Rev-GFP RACE GSP1: 5'-TCA CCC TCT CCA CTG ACA GAG AAC TT-3'). To detect cleavage products, nested PCR was performed using primers complementary to the RNA adaptor (5'-cDNA primer: 5'-GGA CAC TGA CAT GGA CTG AAG GAG TA-3') and gene-specific primer 2 (Rev-GFP RACE GSP2: 5'-TAA CCT CTC AAG CGG TGG TAG CTG AA-3'). Amplification products were resolved using agarose gel electrophoresis and visualized using ethidium bromide staining. Specific PCR products were recovered using a QIAquick Gel purification Kit (Qiagen, Germantown, MD), then were cloned into the TOPO TA cloning vector pCR4-TOPO vector (Thermo Fisher Scientific, Waltham, MA). Individual clones were identified using DNA sequencing.



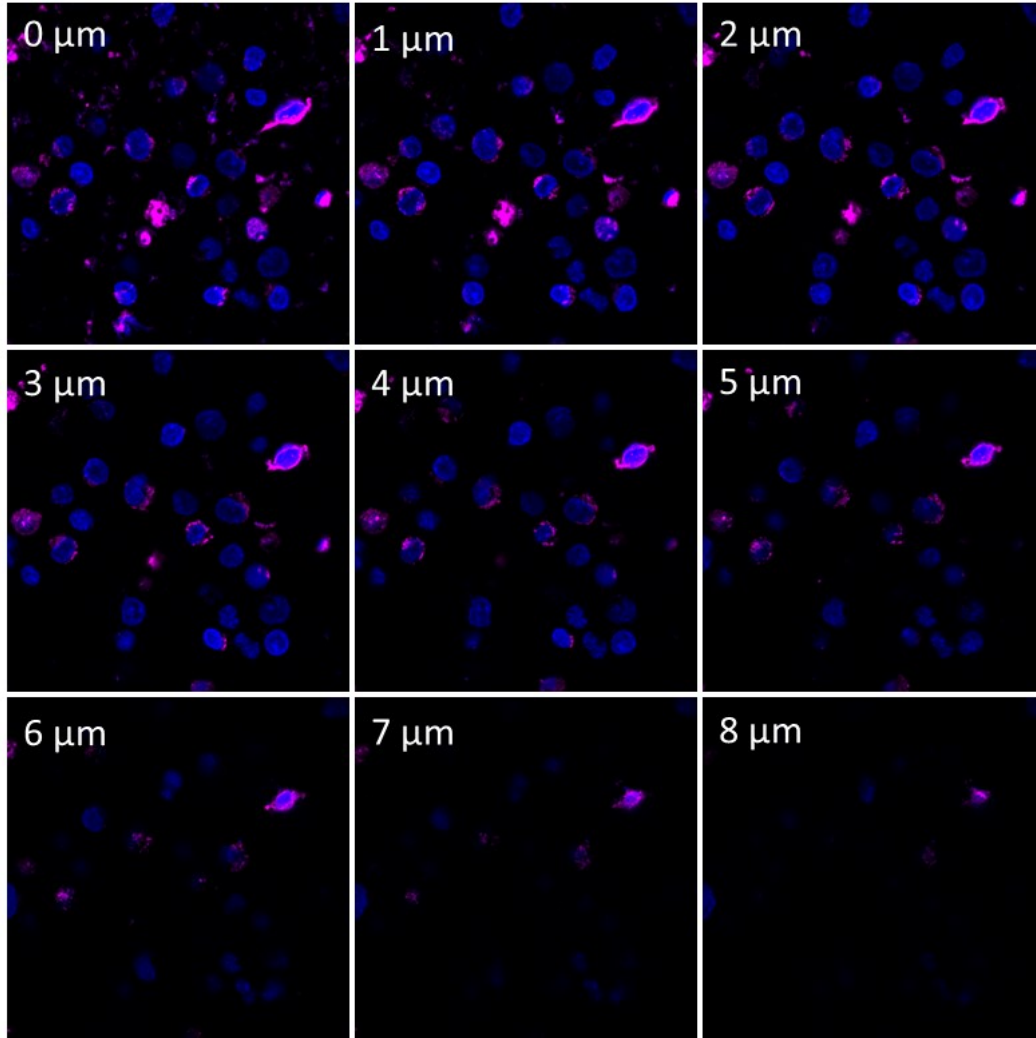


**Figure S1. Real-time live-cell confocal microscopy analysis.** PBMCs were incubated with Cy3-FANA at a final concentration of 100 nM for 4 h. Z-stack images were collected with a step size of 1  $\mu\text{m}$ , as indicated, using 40x magnification. Magenta: Cy3-FANA; Blue: Hoechst 33342.

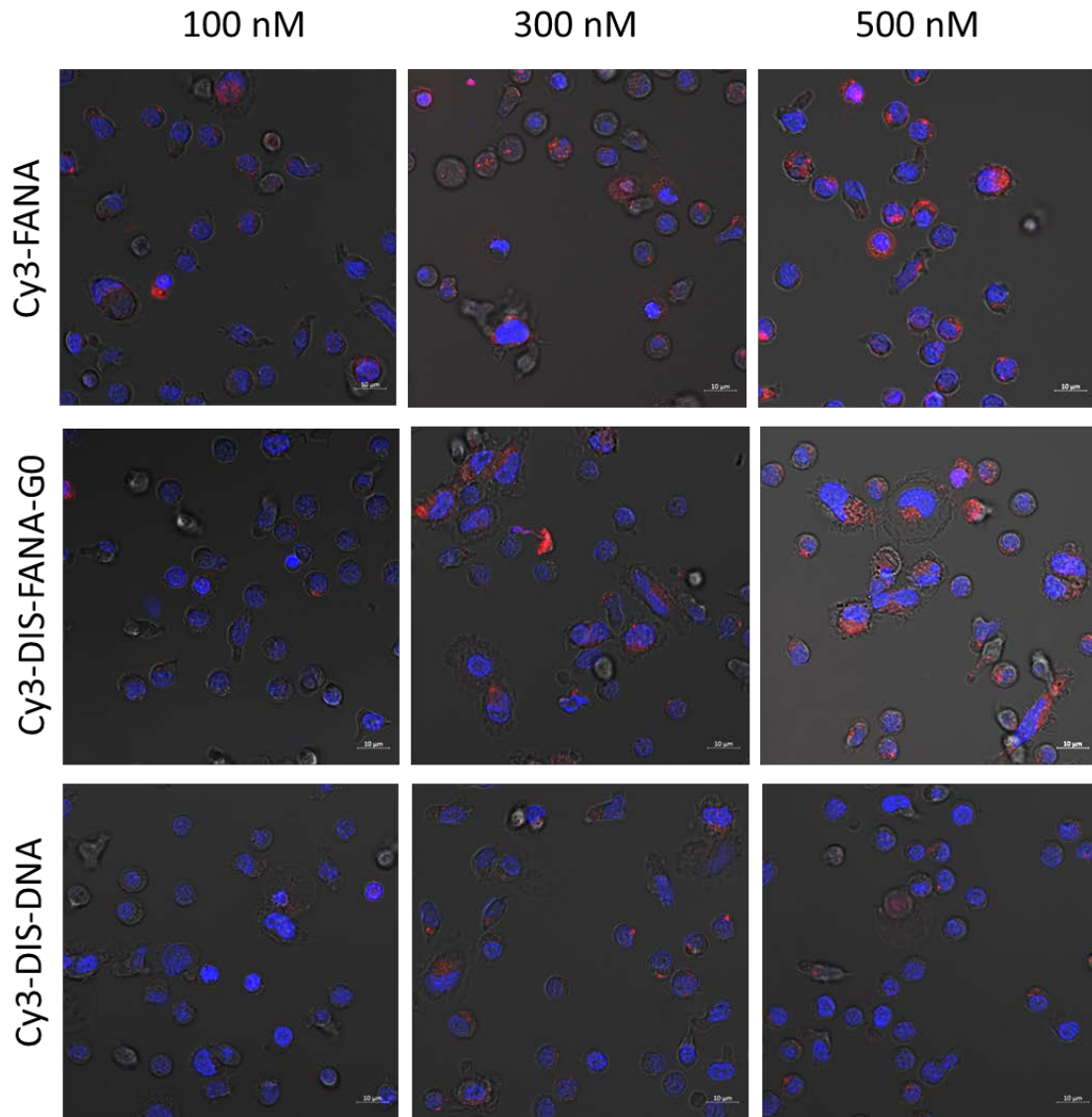


**Figure S2. Real-time live-cell confocal microscopy analysis of carrier-free cellular internalization of ASOs in CD8-depleted PBMCs.** CD8-depleted PBMCs were incubated with Cy3-labeled ASOs at indicated concentrations for 4 h. Representative images were collected using 40x magnification. Red: Cy3-FANA, Cy3-DIS-FANA-G0, or Cy3-DIS-DNA; Blue: Hoechst 33342.

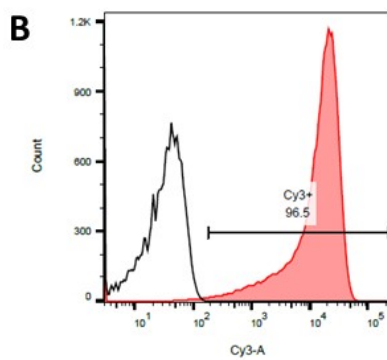
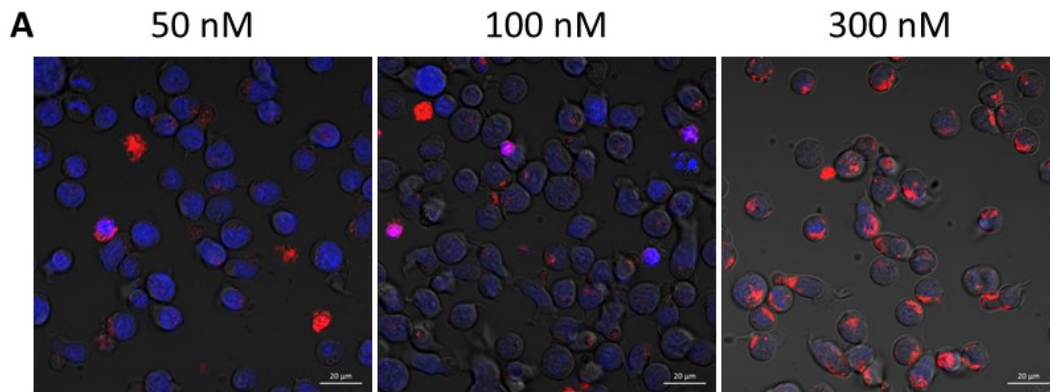


**Figure S3. Carrier-free cellular internalization studies of FANA ASO in CCRF-CEM cells.** (A) Real-time live-cell confocal microscopy analysis. CCRF-CEM cells were incubated with Cy3-FANA at indicated concentrations for 4 h. Representative images were collected using 40x magnification. Red: Cy3-FANA; Blue: Hoechst 33342. (B) Cellular uptake level of Cy3-FANA assessed by flow cytometry. CEM-CCRF cells were incubated with Cy3-FANA at a concentration of 100 nM in complete media for 4 h. After being washed and stained with DAPI, cells were immediately analyzed by flow cytometry.

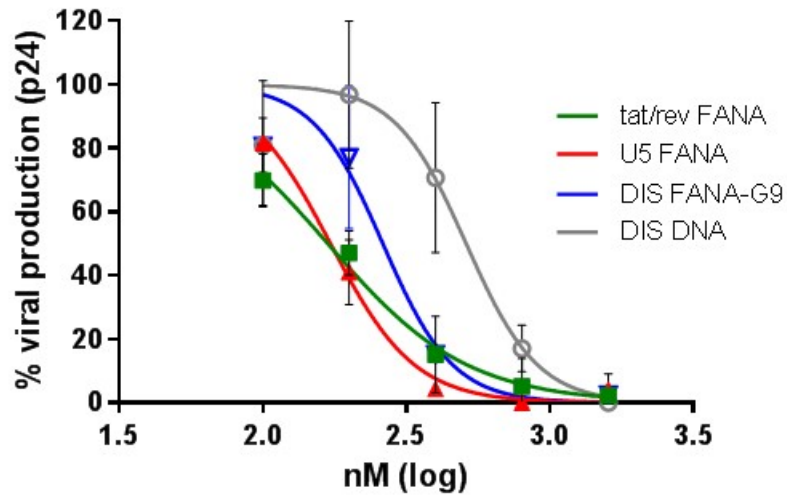


**Figure S4. Dose-response curves for anti-HIV ASOs.** HIV-1<sub>NL4-3</sub>-infected PBMC-CD4<sup>+</sup> T cells were treated with indicated FANA ASOs at final concentrations of 100 nM, 200 nM, 400 nM, 800 nM, or 1600 nM. Data represent the relative viral production level calculated based on HIV-1 p24 expression. All experiments were performed in triplicate and data show mean values from at least three assays, each of which used cells isolated from different donors. Error bars indicate SD.

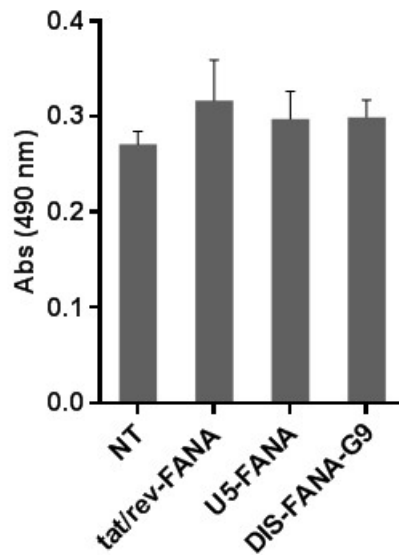


**Figure S5. Effect of FANA ASOs on cell proliferation of PBMCs.** HIV-1<sub>NL4-3</sub>-infected PBMC-CD4<sup>+</sup> T cells were incubated with indicated FANA ASOs at final concentrations of 3  $\mu$ M for 10 days. Cytotoxicity was measured using CellTiter 96<sup>®</sup> AQueous One Solution Cell Proliferation Assay System. All experiments were performed in triplicate and data show mean values and standard deviation from at least three assays, each of which used cells isolated from different donors. Error bars indicate SD.

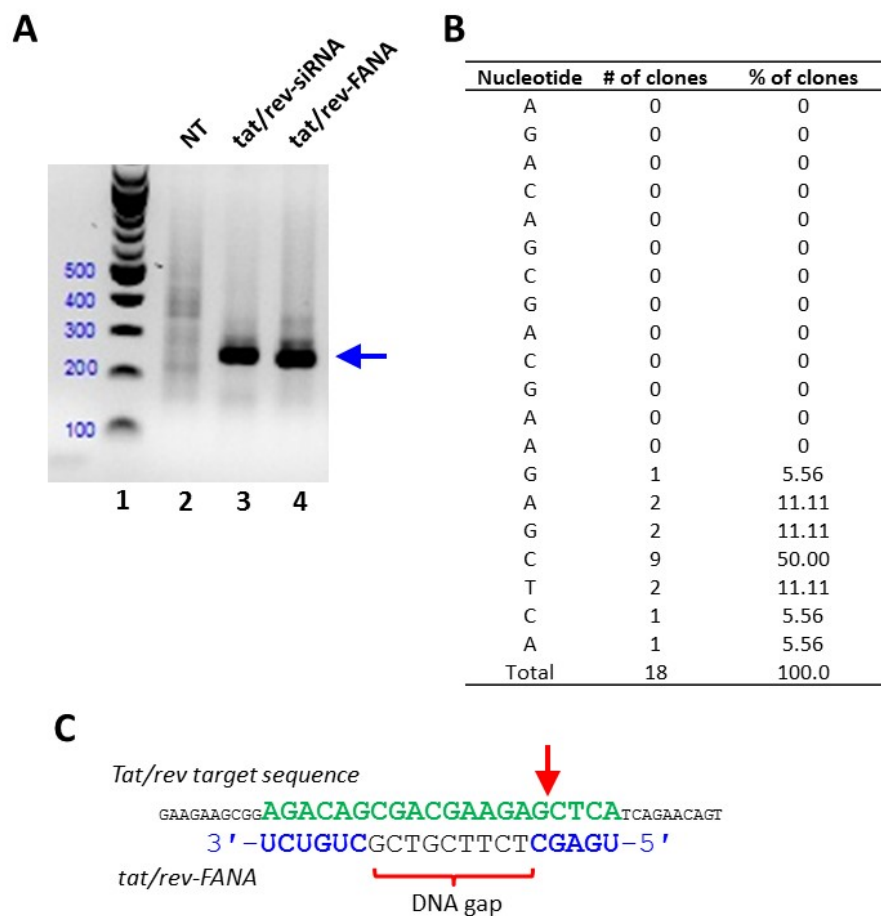


**Figure S6. 5'-RACE PCR analysis of RNase H-mediated cleavage of target RNA.** Tat/rev siRNA or tat/rev-FANA was co-transfected into HEK293T cells with a Rev-EGFP fusion construct harboring the tat/rev target using Lipofectamine2000. After a 48-h incubation, total RNA was isolated from cells, ligated to a GeneRacer adaptor, and reverse transcribed using a gene-specific primer 1. Nested PCR was performed using primers complementary to the RNA adaptor and gene-specific primer 2. (A) Nested PCR products were resolved in an agarose gel. Lane 1: 100 bp DNA ladder; lane 2: NT; lane 3: tat/rev-siRNA; lane 4: tat/rev-FANA. RNase H-mediated cleavage RNA RACE PCR products are marked with a blue arrow. (B and C) DNA sequence analyses of cloned RACE PCR products. The position of the major site of RNase H-mediated cleavage in the tat/rev target RNA is indicated with a red arrow.

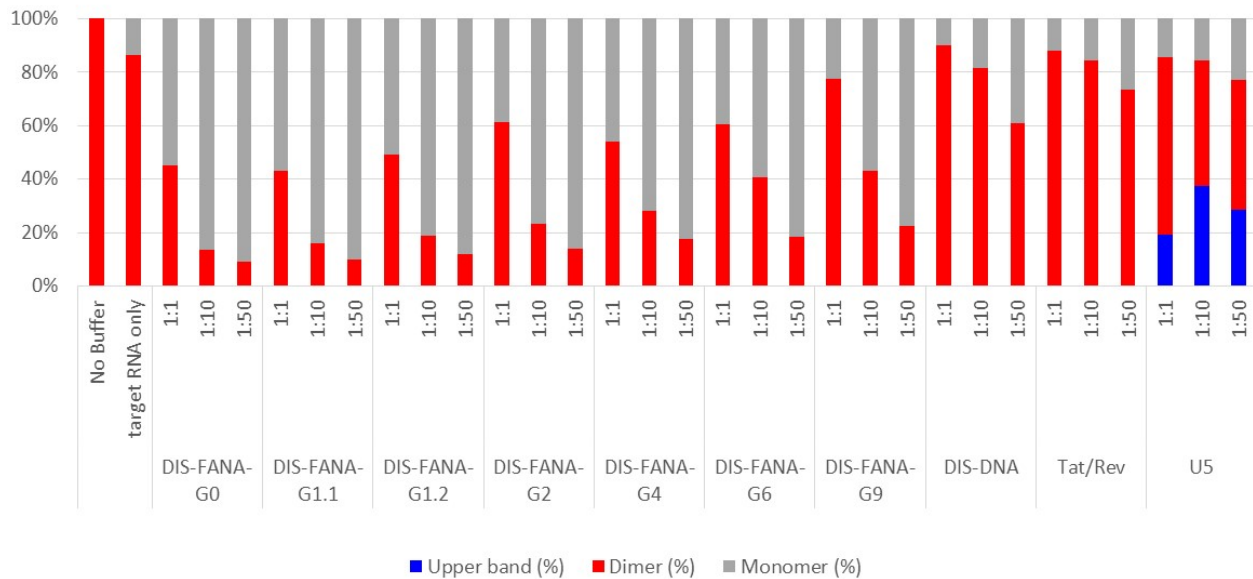


**Figure S7. Inhibition of viral RNA dimerization by DIS-FANA ASOs.** Dimers and monomers were separated by agarose gel electrophoresis (Figure 6). The bands were quantified and plotted as a ratio of the amount of dimer (red), monomer (grey), and unknown product (upper band; blue) to the total amount of the three products (100%).